Applied Physics Letters

Anisotropic electronic phase transition in CrN epitaxial thin films

Cite as: Appl. Phys. Lett. **120**, 073103 (2022); https://doi.org/10.1063/5.0079360
Submitted: 20 November 2021 • Accepted: 02 February 2022 • Published Online: 15 February 2022

Qiao Jin, Jiali Zhao, Manuel A. Roldan, et al.

Applied Physics Letters ARTICLE scitation.org/journal/apl

Anisotropic electronic phase transition in CrN epitaxial thin films

Cite as: Appl. Phys. Lett. **120**, 073103 (2022); doi: 10.1063/5.0079360
Submitted: 20 November 2021 · Accepted: 2 February 2022 ·
Published Online: 15 February 2022

Qiao Jin,[1,2] Jiali Zhao,[1] Manuel A. Roldan,[3] Weiheng Qi,[2,4] Shan Lin,[1,2] Shengru Chen,[1,2] Haitao Hong,[1,2] Yiyan Fan,[1] Dongke Rong,[1] Haizhong Guo,[5] Chen Ge,[1] Can Wang,[1,6] Jia-Ou Wang,[4] Shanmin Wang,[7] Kui-juan Jin,[1,2,6,a)] and Er-Jia Guo[1,2,6,a)]

AFFILIATIONS

[1]Beijing National Laboratory for Condensed Matter Physics and Institute of Physics, Chinese Academy of Sciences, Beijing 100190, China
[2]School of Physical Sciences, University of Chinese Academy of Sciences, Beijing 100190, China
[3]John M. Cowley Center for High Resolution Electron Microscopy, Arizona State University, Tempe, Arizona 85287, USA
[4]Beijing Synchrotron Radiation Facility, Institute of High Energy Physics, Chinese Academy of Sciences, Beijing 100049, China
[5]School of Physics and Microelectronics, Zhengzhou University, Zhengzhou 450001, China
[6]Songshan Lake Materials Laboratory, Dongguan, Guangdong 523808, China
[7]Department of Physics, Southern University of Science and Technology, Shenzhen, Guangdong 518055, China

[a)]**Authors to whom correspondence should be addressed:** kjjin@iphy.ac.cn and ejguo@iphy.ac.cn

ABSTRACT

Electronic phase transition in strongly correlated materials is extremely sensitive to the dimensionality and crystallographic orientations. Transition metal nitrides (TMNs) are seldom investigated due to the difficulty in fabricating high-quality and stoichiometric single crystals. In this Letter, we report the epitaxial growth and electronic properties of CrN films grown on different-oriented $NdGaO_3$ (NGO) substrates. Astonishingly, CrN films grown on (110)-oriented NGO substrates maintain a metallic phase, whereas the CrN films grown on (010)-oriented NGO substrates are semiconducting. We attribute the unconventional electronic phase transitions in CrN films to the strain effects. The effective modulation of bandgap by the anisotropic strain triggers the metal-to-insulator transition consequently. This work provides a convenient approach to modify the electronic ground states of functional materials using anisotropic strain and further stimulates the investigations of TMNs.

Transition metal nitrides (TMNs) exhibit wide applications in the energy and coating fields due to their outstanding thermoelectricity,[1] catalysis,[2,3] and mechanical properties.[4] However, the intrinsic physical properties of TMNs have not been well explored because the fabrication of stoichiometric single-crystalline TMNs is very challenging.[5,6] Among the functional TMNs, chromium nitride (CrN) is an excellent metallic antiferromagnet and is readily applied in the next-generation spintronic and terahertz devices.[7] Bulk CrN has a paramagnetic cubic structure above Néel temperature T_N (~280 K) and transforms to the antiferromagnetic orthorhombic structure below T_N.[8,9] It serves as an alternative option to the well-established antiferromagnetic metallic alloys, such as Mn_3Pt[10] and Mn_2Au,[11,12] because of its low price and robustness in ambient conditions. Therefore, thoughtful understanding of the magnetic and electrical properties of CrN is highly encouraging.

So far, the investigations of transport behaviors of CrN bulk and thin films are contradictory in the studies.[1,9,13–18] Some groups report that CrN maintains semiconducting down to 5 K, while others demonstrate that CrN undergoes an insulator-to-semiconductor transition or an insulator-to-metal transition with a sharp resistivity drop across T_N. These controversial results can be attributed to the crystalline impurities or nitrogen vacancies. Experimentally, it is challenging to fabricate high-quality stoichiometric CrN thin films by magnetron sputtering or laser splatting. The high-energy excited transition metal ions and high-vacuum environment unavoidably introduce the nitrogen deficiency in the as-grown CrN films. Recently, we developed a growth methodology for high-quality TMNs thin films using pulsed laser deposition technique assisted with an atomic nitrogen plasma source.[19] The nitrogen vacancies can be largely suppressed during the film growth. Intrinsic electrical properties can be investigated as a

function of substrate-induced misfit strain and film thickness. The electrical conductivity in CrN maintains when its thickness reduces to one unit cell.[19]

Different from the biaxial strain induced by cubic substrates, single-crystalline thin films epitaxially grown on orthorhombic $NdGaO_3$ (NGO) substrates with various orientations suffer remarkably different in-plane strains. Therefore, the on-site Coulomb electronic correlation and band structure are also affected by the lattice distortion depending on the crystallographic orientation. In this Letter, epitaxial CrN films are coherently grown on NGO substrates with different orientations. Transport properties and electronic states of CrN thin films exhibit remarkable different behaviors. Using x-ray linear dichroism (XLD) measurements, we attribute the anisotropic electronic phase transition in CrN films to the strain-mediated electron redistribution between e_g and t_{2g} orbitals.

The CrN thin films with thickness of ~25 nm were deposited on NGO substrates with (001)-, (010)-, and (110)-orientations (Hefei Kejing Co., Ltd). To avoid nitrogen vacancies in CrN films, we used a stoichiometric ceramic CrN target for laser ablation. The ceramic CrN was synthesized using a high-pressure reaction route. The heating process is carried out at 5 GPa and 1200 °C for 5 min. The powder was then sintered into a target with a diameter of 1 inch at 5 GPa and 1100 °C for 50 min.[20] Previously, we had determined the valence state of Cr ions to be +3 in CrN using x-ray absorption and x-ray photoemission spectroscopy. No apparent nitrogen vacancy was observed in the as-grown CrN films. The metallic phase maintains down to 5 K, and phase transition occurs around ~280 K, indicating that CrN films are clearly stoichiometric. We keep the optimal growth conditions used in our previous work.[19,21] The growth temperature is 600 °C, and the laser frequency and energy density are 5 Hz and ~1.5 J/cm^2, respectively. The CrN films were fabricated in vacuum to avoid oxidization. An atomic nitrogen plasma source was used to compromise the nitrogen vacancies during the deposition. The growth rate was calculated by fitting the x-ray reflectivities; meanwhile, the film thickness was accurately controlled by counting the number of laser pulses.

The structural characterizations of CrN films were performed on a Panalytical X'Pert3 MRD high-resolution diffractometer and at Beijing Synchrotron Radiation Facility. Figure 1(a) shows synchrotron x-ray diffraction (XRD) θ-2θ scans of CrN films grown on NGO substrates with different orientations. Clearly, all CrN films show single phase. The CrN films grown on (001)- and (110)-oriented NGO substrates exhibit (001) orientation, whereas the CrN films on (010)-oriented NGO substrates are (111)-oriented. The striking results are attributed to the minimization of misfit strains between CrN films and NGO substrates (supplementary material Fig. S1). CrN has a cubic rock salt structure where its lattice parameter is $a = 4.15$ Å, while NGO has an orthorhombic structure with *pbnm* space group where its lattice parameters are $a = 5.42$ Å, $b = 5.50$ Å, and $c = 7.71$ Å. When CrN arranges along (001) orientation, the in-plane lattice parameters match to that of pseudocubic NGO (110) ($a_{(110)\,pc} \sim 3.868$ Å), and to that of pseudocubic NGO (001) ($a_{(001)\,pc} \sim 3.848$ Å). The lattice mismatches between CrN and NGO substrates are −6.7% and −7.0% for (110)- and (001)-oriented NGO, respectively. A larger compressive misfit strain from (001)-oriented NGO results in a deteriorated crystallinity of CrN film as evidenced by a weaker diffraction peak intensity. However, when viewed along the [111] direction, CrN presents a hexagonal structure. The Cr^{3+} ions located in the vertex, which is close to that of Nd^{3+} and Ga^{3+} enclosed in (100)- and (010)-oriented NGO. The distances between two nearby transition metal ions are 2.93 and 2.715 Å in (111)-oriented CrN and pseudocubic (010)-oriented NGO, respectively. Therefore, the CrN films grown on (010)-oriented NGO substrates will preferentially arrange along (111)-orientation, yielding to an extremely large compressive strain up to −7.3%.

Reciprocal space mappings around the substrates' 103 peaks [Figs. 1(b) and 1(c)] were performed to determine the in-plane strains of CrN films. The CrN(111) and CrN(001) films have in-plane lattice

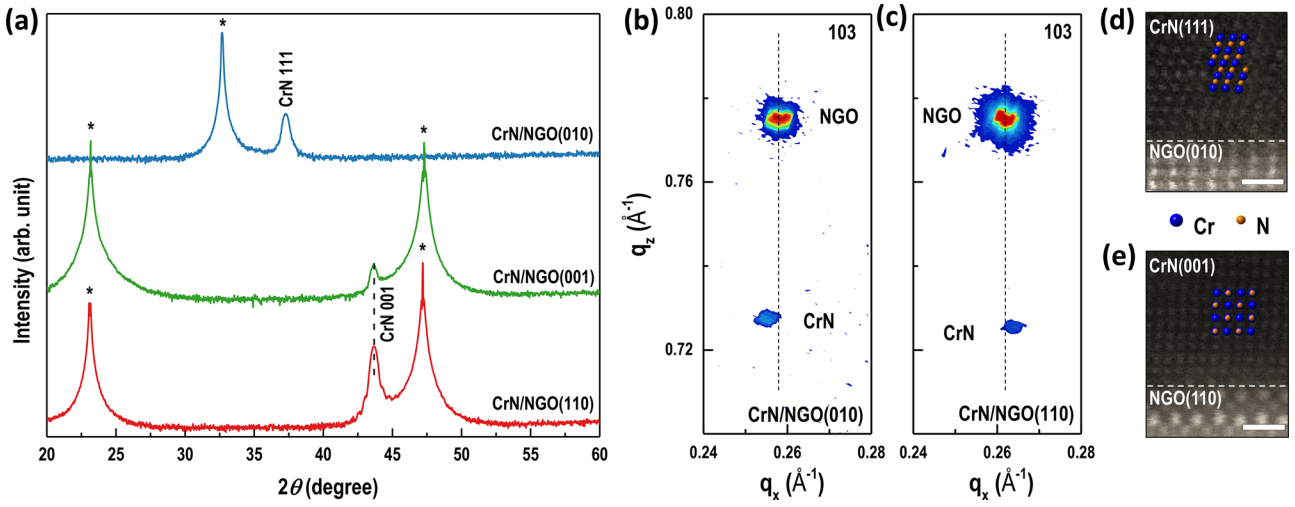

FIG. 1. Structural characterizations of CrN films grown on the different-oriented NGO substrates. (a) Synchrotron XRD θ-2θ scans of 25-nm-thick CrN films grown on (010)-, (001)-, and (110)-oriented NGO substrates. The asterisk symbols (*) indicate the diffraction peaks of NGO substrates. (b) and (c) Reciprocal space mappings around the substrates' 103 peaks for CrN films grown on NGO substrates with (010) and (110) orientations, respectively. (d) and (e) High-magnified HAADF-STEM images of CrN films grown on (010)- and (110)-oriented NGO substrates, respectively. The dashed lines indicate the abrupt interfaces between CrN and NGO.

parameters of 3.90 ± 0.03 and 3.84 ± 0.03 Å, respectively. The in-plane compressive strains of CrN films slightly relax when CrN film thickness reaches to ~25 nm. We find that the crystallinities of CrN films are deteriorated compared to the CrN films grown on MgO substrates with small tensile strains (supplementary material Fig. S2).[19] Figures 1(d), 1(e), and S3 show the high-angle annular dark-field (HAADF) scanning transmission electron microscopy (STEM) images for CrN films grown on (010)- and (110)-oriented NGO substrates, respectively. Both samples exhibit sharp interfaces between films and substrates. The epitaxial relationships were further confirmed by measuring x-ray pole figures around {111} peaks of CrN and NGO (supplementary material Figs. S4 and S5).

To explore the transport properties of the CrN films, we measured temperature dependent resistivity (ρ) using the standard van der Pauw method. All measurements were performed by a physical property measurement system (PPMS). Figure 2(a) shows the ρ-T curves for CrN films with various orientations. All CrN films show the low resistivities (ρ = 0.82–2.26 mΩ·cm) at room temperature, which are comparable to the results from other reports.[1,13,17] Strikingly, we observe a sharp difference in the transport behaviors of CrN films with different orientations. For (001)-oriented CrN films, the metallic states appear at room temperature. As the temperature decreasing, they undergo a metal-to-insulator transition (MIT). T_{MIT} for the CrN films grown on the (110)- and (001)-oriented NGO substrates are 70 and 150 K, respectively. However, the insulating phase in the CrN films grown on the (010)-oriented NGO substrates maintains throughout the measured temperature range. We find that the ρ–T curves of all films cannot be described using a single activated model [$\ln(\rho) \sim 1/T$] or a single Mott's variable range hopping (VRH) model [$\ln(\rho) \sim (1/T)^n$].[17] Previously, Catalan *et al.*[22] combine the normal activated conduction and 3D Mott's VRH to explain the complex transport behaviors,

$$\rho(T) = \rho_0 + A\exp\left(\frac{\Delta E}{k_B T}\right) + B\exp\left[\left(\frac{T_0}{T}\right)^{\frac{1}{4}}\right], \quad (1)$$

where ρ_0, A, and B are constants and T_0 is the temperature normalization constant. The second term describes the thermal excitation: $\rho(T) \sim \exp(\frac{\Delta E}{k_B T})$, where k_B is Boltzmann constant and ΔE is the activation energy. The third term dominates the VRH: $\rho(T) \sim \exp[(\frac{T_0}{T})^m]$, where the index $m = 1/4$ or $m = 1/3$ for three- or two-dimensional VRH. Figures 2(b) and 2(c) show excellent fits for CrN films grown on (110)- and (001)-oriented NGO substrates. We obtain $\Delta E \sim 49.5$ and ~52.6 meV for CrN films grown on (110)- and (001)-oriented NGO substrates, respectively. The increase in bandgap with compressive strain is also consistent with our earlier works.[15,17] As shown in Fig. 2(d), the ρ-T curve of (111)-oriented CrN films follows Eq. (1) below 125 K (solid black line); however, it transits to 2D Mott's VRH above 125 K (solid white line). Simultaneously, we find that ΔE (~55.2 meV) of (111)-oriented CrN films is larger than those of (001)-oriented CrN films.

Meanwhile, the room-temperature Hall mobility (μ) and carrier density (n) of CrN films are obtained. The CrN films exhibit a comparable $n \sim 1 \times 10^{20}$ cm^{-3}. The CrN films grown on (110)-oriented NGO substrates show a maximum μ of 59.3 cm^2·V^{-1}·s^{-1}, and CrN films grown on (010)-oriented NGO substrates have the lowest

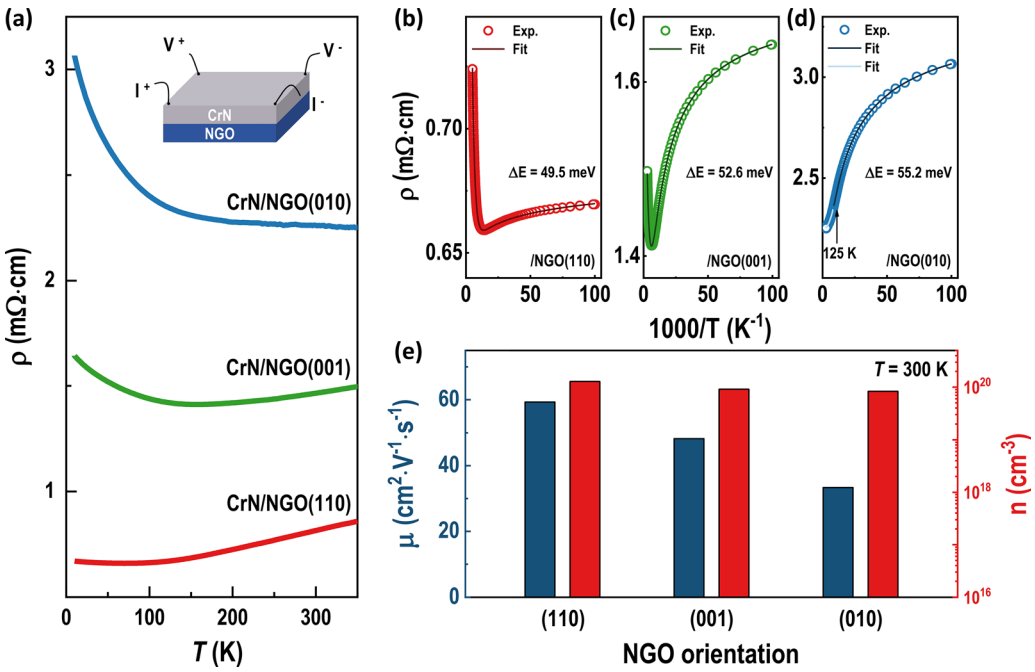

FIG. 2. Transport properties of CrN films. (a) ρ–T curves of CrN films grown on (010)-, (001)-, and (110)-oriented NGO substrates. Inset: schematic of electrical measurements using a conventional van der Pauw method. (b)–(d) Fitted curves of ρ-(1000/T) for CrN films grown on (110)-, (001)-, and (010)-oriented NGO, respectively. (e) Room-temperature carrier mobility (μ) and density (n) for CrN films.

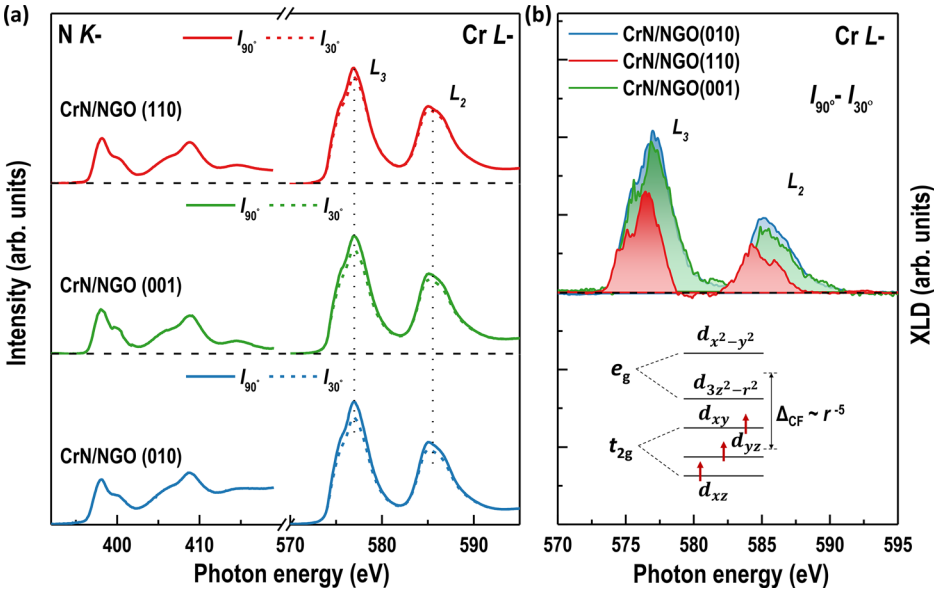

FIG. 3. Electronic state of CrN films. (a) XAS and (b) XLD at N *K*- and Cr *L*-edges for CrN films grown on (110)-, (001)-, and (010)-oriented NGO substrates. XAS were collected with x-ray beam aligned with angles (α) of 90° and 30° respect to the sample's surface. When the $\alpha = 90°$, i.e., the polarization of x-ray is parallel to the in-plane direction, the XAS reflects the $d_{x^2-y^2}$ orbital occupancy ($I_{ip} = I_{90°}$). When the $\alpha = 30°$, XAS probes the unoccupied states in both $d_{x^2-y^2}$ and $d_{3z^2-r^2}$ orbitals, with $I_{oop} = [I_{90°} - I_{30°} \cdot \sin^2 30°)/\cos^2 30°]$. For simplifying the calculations, the signal of $(I_{90°} - I_{30°})$ can indirectly reflect the orbital asymmetry of e_g band and is roughly proportional to the exact XLD signals. Inset: schematic diagram of Cr: *d* orbitals in CrN. The crystal field splitting energy (Δ_{CF}) is inversely proportional to the distance (*r*5) between two Cr atoms.

μ (48.2 $cm^2 \cdot V^{-1} \cdot s^{-1}$). These results suggest that strain-mediated lattice distortion affects the electron scattering in CrN films even though the number of itinerant electrons keeps almost constant independent of crystallographic orientations.

To explore the intrinsic strain effect on the electronic states, we performed the x-ray absorption spectroscopy (XAS) and XLD measurements on CrN films at N *K*- and Cr *L*-edges at room temperature. As shown in Fig. 3(a), the centroid of Cr L_3 peak for all CrN films is ~577.0 eV, and the line shape and peak positions of N *K*-edges are consistent with those of other epitaxial CrN films.[15,19] These results suggest that the valence state of Cr ions is 3+, and the CrN films are stoichiometric with negligible nitrogen vacancies. The XLD measurements were performed using x-ray beam aligned with angles (α) of 90° and 30° with respect to the sample's surface [Fig. 3(b)]. When $\alpha = 90°$, i.e., the polarization of x-ray is parallel to the in-plane direction, and the XAS signal reflects the $d_{x^2-y^2}$ orbital occupancy ($I_{ip} = I_{90°}$). When $\alpha = 30°$, XAS probes the unoccupied states in both $d_{x^2-y^2}$ and $d_{3z^2-r^2}$ orbitals, with $I_{oop} = [I_{90°} - I_{30°} \cdot \sin^2 30°)/\cos^2 30°]$. For simplifying the calculations, the signal of $(I_{90°} - I_{30°})$ can indirectly reflect the orbital asymmetry of e_g band and is roughly proportional to the exact XLD signals. All CrN films exhibit the positive XLD values, suggesting a higher occupancy in the $d_{3z^2-r^2}$ orbitals compared to that of the $d_{x^2-y^2}$ orbitals. The peak values of XLD scale with compressive strain. Inset of Fig. 3(b) shows the schematic of Cr: *d* orbitals in CrN. The degenerated orbitals split into the upper two-fold e_g bands ($d_{x^2-y^2}$ and $d_{3z^2-r^2}$) and the lower threefold t_{2g} bands (d_{xz}, d_{yz}, and d_{xy}). Three electrons fill into the t_{2g} bands with one electron filled into the d_{xz}, d_{yz}, and d_{xy} orbitals. The upper-energy $d_{x^2-y^2}$ and $d_{3z^2-r^2}$ orbitals are empty.[23] The compressive strain will reduce the atomic distance (*r*) between Cr ions, leading to an increase in Δ_{CF} accordingly. As increasing compressive strain, the occupancy of itinerant electrons reduces; thus, the conductivity of CrN films decreases. The localization of free carriers triggers the phase transition in CrN films grown on (010)-oriented NGO substrates. Similarly, in our previous work, the strain-mediated electronic anisotropy and electron redistribution within degenerated orbitals were also revealed in $SrFeO_2$ films grown on various substrates.[24] Furthermore, the reduced conductivity and electronic phase transition in (111)-oriented CrN films may also be related to the differences in the film quality. The larger compressive strain results in a higher defect density in CrN(111) films; thus, an insulating state appears in contrast to the metallic state in CrN(001) films.

In summary, we fabricated a series of high-quality CrN thin films on different-oriented NGO substrates. The crystallographic arrangement and transport behaviors of CrN films strongly depend on the substrates' orientations. The (001)-oriented CrN films exhibit a MIT as decreasing the temperature, whereas the (111)-oriented CrN maintains its insulating phase. We attribute the intriguing phase transition in CrN films to the strain-mediated electronic band structures. The compressive strain increases the bandgap and enhances the itinerant electron scattering, leading to the CrN transforming from the 3D metallic state to the 2D insulating state. Our results strengthen the important role of epitaxial strain in the intrinsic physical properties in TMNs and unquestionably stimulate the investigation of TMNs toward electronic devices.

See the supplementary material for additional information about the crystallographic epitaxial relationship, reciprocal space mappings, pole figures, and large-scale STEM measurements.

This work was supported by the National Key Basic Research Program of China (Grant Nos. 2020YFA0309100 and 2019YFA0308500), the National Natural Science Foundation of China (Grant Nos. 11974390, 52025025, and 52072400), the Beijing Nova Program of Science and Technology (Grant No. Z191100001119112), the Beijing Natural Science Foundation (Grant No. 2202060), the Guangdong-Hong Kong-Macao Joint Laboratory for Neutron Scattering Science and Technology, and the Strategic Priority Research Program (B) of the Chinese Academy of Sciences (Grant No. XDB33030200).

The XAS and XRD experiments at the beam line 4B9B and 1W1A of the Beijing Synchrotron Radiation Facility (BSRF) of the Institute of High Energy Physics, Chinese Academy of Sciences, were conducted via a user proposal. The authors acknowledge the use of facilities within the Eyring Materials Center at Arizona State University.

AUTHOR DECLARATIONS

Conflict of Interest

The authors have no conflicts to disclose.

DATA AVAILABILITY

The data that support the findings of this study are available from the corresponding authors upon reasonable request.

REFERENCES

[1]C. X. Quintela, J. P. Podkaminer, M. N. Luckyanova, T. R. Paudel, E. L. Thies, D. A. Hillsberry, D. A. Tenne, E. Y. Tsymbal, G. Chen, C. B. Eom, and F. Rivadulla, Adv. Mater. **27**, 3032–3037 (2015).
[2]X. Xiao, X. Peng, H. Jin, T. Li, C. Zhang, B. Gao, B. Hu, K. Huo, and J. Zhou, Adv. Mater. **25**, 5091–5097 (2013).
[3]Y. Shi, Y. Wan, R. Zhang, and D. Zhao, Adv. Funct. Mater. **18**, 2436–2443 (2008).
[4]B. D. Fulcher, X. Y. Cui, B. Delley, and C. Stampfl, Phys. Rev. B **85**, 184106 (2012).
[5]W. Sun, C. J. Bartel, E. Arca, S. R. Bauers, B. Matthews, B. Orvananos, B. R. Chen, M. F. Toney, L. T. Schelhas, W. Tumas, J. Tate, A. Zakutayev, S. Lany, A. M. Holder, and G. Ceder, Nat. Mater. **18**, 732–739 (2019).
[6]J. M. D. Coey and P. A. I. Smith, J. Magn. Magn. Mater. **200**, 405–424 (1999).
[7]R. Morales, Z. P. Li, J. Olamit, K. Liu, J. M. Alameda, and I. K. Schuller, Phys. Rev. Lett. **102**, 097201 (2009).
[8]L. M. Corliss, N. Elliott, and J. M. Hastings, Phys. Rev. **117**, 929–935 (1960).
[9]K. Inumaru, K. Koyama, N. Imo-oka, and S. Yamanaka, Phys. Rev. B **75**, 054416 (2007).
[10]Z. Q. Liu, H. Chen, J. M. Wang, J. H. Liu, K. Wang, Z. X. Feng, H. Yan, X. R. Wang, C. B. Jiang, J. M. D. Coey, and A. H. MacDonald, Nat. Electron. **1**, 172–177 (2018).
[11]V. M. Barthem, C. V. Colin, H. Mayaffre, M. H. Julien, and D. Givord, Nat. Commun. **4**, 2892 (2013).
[12]X. Chen, X. Zhou, R. Cheng, C. Song, J. Zhang, Y. Wu, Y. Ba, H. Li, Y. Sun, Y. You, Y. Zhao, and F. Pan, Nat. Mater. **18**, 931–935 (2019).
[13]D. Gall, C. S. Shin, R. T. Haasch, I. Petrov, and J. E. Greene, J. Appl. Phys. **91**, 5882–5886 (2002).
[14]C. Constantin, M. B. Haider, D. Ingram, and A. R. Smith, Appl. Phys. Lett. **85**, 6371–6373 (2004).
[15]P. A. Bhobe, A. Chainani, M. Taguchi, T. Takeuchi, R. Eguchi, M. Matsunami, K. Ishizaka, Y. Takata, M. Oura, Y. Senba, H. Ohashi, Y. Nishino, M. Yabashi, K. Tamasaku, T. Ishikawa, K. Takenaka, H. Takagi, and S. Shin, Phys. Rev. Lett. **104**, 236404 (2010).
[16]X. Y. Zhang, J. S. Chawla, R. P. Deng, and D. Gall, Phys. Rev. B **84**, 073101 (2011).
[17]X. Y. Zhang, J. S. Chawla, B. M. Howe, and D. Gall, Phys. Rev. B **83**, 165205 (2011).
[18]X. F. Duan, W. B. Mi, Z. B. Guo, and H. L. Bai, J. Appl. Phys. **113**, 023701 (2013).
[19]Q. Jin, H. Cheng, Z. Wang, Q. Zhang, S. Lin, M. A. Roldan, J. Zhao, J. O. Wang, S. Chen, M. He, C. Ge, C. Wang, H. B. Lu, H. Guo, L. Gu, X. Tong, T. Zhu, S. Wang, H. Yang, K. J. Jin, and E. J. Guo, Adv. Mater. **33**, 2005920 (2021).
[20]S. Wang, X. Yu, J. Zhang, L. Wang, K. Leinenweber, D. He, and Y. Zhao, Cryst. Growth Des. **16**, 351–358 (2016).
[21]Q. Jin, Z. Wang, Q. Zhang, J. Zhao, H. Cheng, S. Lin, S. Chen, S. Chen, H. Guo, M. He, C. Ge, C. Wang, J.-O. Wang, L. Gu, S. Wang, H. Yang, K.-J. Jin, and E.-J. Guo, Phys. Rev. Mater. **5**, 023604 (2021).
[22]G. Catalan, R. M. Bowman, and J. M. Gregg, Phys. Rev. B **62**, 7892–7900 (2000).
[23]A. S. Botana, V. Pardo, D. Baldomir, and P. Blaha, Phys. Rev. B **87**, 075114 (2013).
[24]S. Chen, J. Zhao, Q. Jin, S. Lin, S. Chen, H. Yao, J. Wang, Z. Fan, E. Guo, and H. Guo, Sci. China-Phys. Mech. Astron. **64**, 287711 (2021).